MECHANICAL BEHAVIOR OF CORN STALK PITH: AN EXPERIMENTAL AND MODELING STUDY
/
玉米秸秆内瓤的力学特性试验与模拟研究

Lect.Ph.D. Stud. Lixian Zhang [1)], Prof. Ph.D. Zhongping Yang *[1)], Prof. Ph.D. Eng. Qiang Zhang [2)], Prof. Xinhua Zhu [1)], Lect.Ph.D.Haijun Hu [3)]
[1)] Department of Mechanical and Electronic Engineering, Northwest A&F University, Shaanxi/China;
[2)] Department of Biosystems Engineering, University of Manitoba, Manitoba /Canada;
[3)] College of Water Resources and Architectural Engineering, Northwest A&F University, Shaanxi/China
Tel: +8613384943185; E-mail: zhanglixian031229@126.com

Keywords: *corn stalk pith, mechanical properties, discrete element model (DEM), tensile strength*

ABSTRACT

Corn stalk pith (CSP) is porous and highly elastic, which makes it an excellent renewable packaging material with good cushioning properties. This paper investigated some important mechanical properties of corn stalk pith. The effects of moisture content, internodal position and variety on corn stalk pith's tensile strength and the Young's modulus were experimentally determined. A discrete element model (DEM) was developed to simulate the tensile testing process. It was found that the mechanical properties of corn stalk pitch were highly variable, with a tensile strength in the range of 0.2-1.35MPa, and Young's modulus 0.02-0.19GPa. The tensile strength of CSP increased with moisture content, while the Young's modulus showed the opposite tendency. From the DEM simulations of the load-displacement curve of CSP, the values of key mechanical properties in the DEM were determined: the normal stiffness coefficient k_n = (0.5-3) x 10^6 N/m; the tangent stiffness coefficient k_s= 1.0x10^6N/m; the normal bonding coefficient n-bond = (5-50) N/m^3; and the tangential bonding coefficient s-bond = (10-50) N/m^3. These values provided important and necessary data for further analysing the mechanical properties of packaging materials made of CSP.

摘要

玉米秸秆内穰细胞疏松多孔、弹性大，是缓压减震包装材料的一种主要原材料，其力学特性对包装材料的强度等性能指标具有重要影响。本文对玉米秸秆内穰的拉伸特性进行深入探究；测试了含水率、节间位置及品种对玉米秸秆内瓤抗拉强度和弹性模量的影响；建立离散元模型模拟了拉伸过程中的力学行为。研究结果表明：随含水率增加秸秆内瓤的抗拉强度增大，而弹性模量减小；秸秆内穰抗拉强度为0.2-1.35MPa，弹性模量为 0.02-0.19GPa。在设定的含水率下，模拟得到了玉米秸秆内穰拉伸变形图和载荷位移曲线，获得了离散元模型的主要力学特性参数：法向刚度系数 Kn=（0.5-3）×10^6 N/m，切向刚度系数 Ks=1.0×10^6N/m，法向粘合系数 n-bond=(5-50)N/m^3，切向粘合系数 s-bond=(10-50)N/m^3。上述研究结果为分析和确定基于秸秆内穰的包装材料性能指标提供理论参考。

INTRODUCTION

Corn stalk is an important renewable resource. A lot of research and exploration of the potential usage of corn stalk have been conducted *(Husseien M. et al., 2009; Igathinathane C. et al., 2010; Li Zhiyong et al., 2012)*. Corn stalk has complex mechanical properties, due to its inhomogeneous compositions and structures. For example, corn stalk rind has high lignin content and strength, which makes it a good raw material for making paper and biocomposites *(Speck Thomas et al., 2011)* . In contrast, corn stalk pith (CSP) is porous and highly deformable, and thus uniquely suited as a good cushioning packaging material *(Rousserie F et al., 1997)*. To fully explore the potential of corn stalk pith as a "green" material for industrial usage, the knowledge of mechanical properties of CSP is critical, such as the strength and elasticity. These properties dictate the performance of final products derived from CSP, as well as equipment design for processing CSP. For example, damages of pith structure during processing may affect the packaging material's effectiveness. Limited information exists in the literature on the mechanical properties of CSP. The objectives of this study were to: (1) determine several critical mechanical property parameters, such as the tensile strength and Young's modulus, as affected by moisture content, intermodal position for different corn varieties; and (2) develop a discrete element model (DEM) to simulate mechanical behaviour of CSP.

Many studies of the mechanical properties of corn stalk have been conducted to explore the potential use of this renewable material. Reddy, et al.*(Reddy Narendra et al., 2005)* investigated the structure of corn stalk rind fibre using a tensile tester, X-ray diffraction and a scanning electron microscope. Their tensile test

results showed that the tensile strength range was 1.5-4.5g per denier. Rodriguez, et al.*(Panthapulakkal Suhara et al., 2007; Rodriguez Manuel et al., 2010)* derived the intrinsic tensile strength of the polypropylene composites that constitute the corn stalk; The tensile tests conducted in their study showed corn stalks strength to be 460-670 *MPa*. Von, et al.*(Von Forell Greg et al., 2015)* studied the influence of structure and moisture content on the mechanical properties of corn stalk and determined the ultimate strength and the Young's modulus. Their study was based on simulations of a finite element model (FEM), and the results revealed that the diameter of the corn stalk had a significant impact on the bending strength. The results also suggested a new strategy for breeding and developing maize varieties for producing bioenergy, specifically, counterbalancing tissue weaknesses by relatively small increases (e.g. 5%) in stalk diameter that reduced structural stresses. Hu, etc.*(Hu H. et al., 2013; Peiffer Jason A et al., 2013; Zhong-Zhen Sun et al., 2013)* conducted three and four points bending tests to measure the bending strength and Young's modulus of corn stalk and developed a viscoelastic model. They concluded that the viscoelasticity of corn stalks was closely related to the corn stalk variety, moisture content and intermodal position. Zhang, et al.*(Zhang L. et al., 2016)* measured the average values of Young's modulus and tensile strength of corn stalk rind to be 122.26 MPa and 19.31 *GPa*, respectively. Chen, et al. determined the tensile strength of corn stalk rind to be 67.2MPa *(Chen Zhengguang et al., 2012)*. Huang, et al.*(Liao Na. et al. 2011)* measured corn stalk pith's viscoelastic coefficient in a transverse compression experiment and developed a FEM model to simulate the compression and stress relaxation processes.

Corn stalk pith is porous and voids in the structure frequently occur after the material is dried. Studies *(Wang Donghai et al., 2002)* have shown that the mechanical properties of corn stalk pith are highly related to its microstructure. This means that the models for porous materials, such as DEM, would be better suited for capturing the effect of microstructure of corn stalk pith. The DEM models have been utilized to model the mechanical behaviours of porous materials, such as soil, rock and concrete *(Cundall Peter A, 1988; Hart R. et al., 1988; Qin Chuan et al., 2013)*. Based on an intensive literature review, we know that corn stalk pith may be approximated by bonding discrete spherical particles that represent the porous corn stalk pith. This paper focuses on the development of a discrete dynamic model for corn stalk pith using commercial DEM software and an experimental validation of the simulation results by means of a tensile testing experiment.

The remainder of this paper is organized as follows. Section 3 describes the corn stalk pith tensile tests, presents the tensile test method and process. Section 4 focuses on the development of the DEM model. It explains discrete element contacting theory; introduces the setup of the model, including the creation of the geometry model and mechanical parameters; Section 5 presents the tensile test results, analyses the influence of related parameters on the results, and compares both the simulation and the experimental results. The final section summarizes our findings from the comparison of the simulation and experimental results.

MATERIAL AND METHODS

Tensile tests

The corn stalk samples were obtained from an experimental plot at the Northwest A&F University, Yangling, China. This plot was planted in June, 2013 and harvested in October, 2013. The plant height was approximately 180-220 cm. Each plant had at least nine internodes that were fully grown and was representative of all corn stalks in the same plot. The leaves were removed from the corn stalks and the rinds were peeled off. The dumb-bell shaped specimens were cut out of corn stalks manually. All tensile specimens had an overall dimension of 90 mm x 2 mm x 15 mm (length x thickness x width); the width at the narrow section in the middle was 5 mm, and there was a 50-mm test section between the grips (Fig. 1).

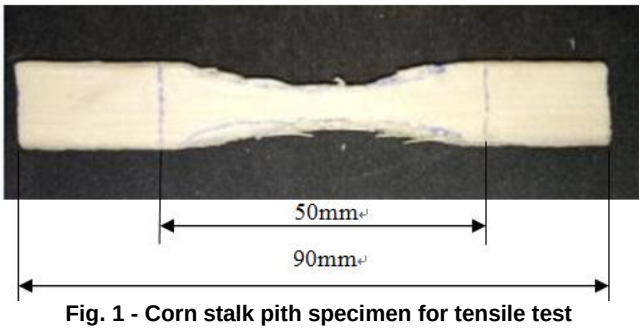

Fig. 1 - Corn stalk pith specimen for tensile test

The conditions of specimens, such as moisture content, would have significant impact on the mechanical properties of CSP. Three important sample conditions were considered in this study, as summarized in Table 1 *(Nazari Galedar M. et al., 2008; Tavakoli H et al., 2009)*. The samples from two corn varieties, SD9 and SD12, were tested.

Table 1

Conditions of CSP test specimens

Factor	Level	Details
Moisture content	10%(dry)	Natural drying > 3 month
	70%(fresh)	Less than 3 hours after being cut
Internodes position	1—9	9 internodes from root to top

Tests were conducted using a biomechanical testing machine (Fig.2, Changchun Machinery Research Institute, Changchun, Liaoning China). The test machine had a capacity of 10 KN, with a force measurement accuracy of ± 0.5%, and movement accuracy of ±0.02%. The specimen was installed on the test machine by using a pair of grips (Fig.2). A computer data acquisition system recorded the magnitude of the applied load to the specimen and elongation of the specimen.

Fig. 2 - Biomechanical testing machine

The tests were conducted following the ASTM Standards*(Astm, 2014)* (Tensile strength, Young's modulus, stress-strain measurement method for steel material). The moisture content was measured according to the ASABE standard*(Asbe, 2006)*. A loading speed of 5 mm/min was used for all tests to minimize the loading rate effect *(Wright Christopher T et al., 2005).*

The stress-strain curve was plotted directly from the data post-processing software associated with the biomechanical tensile tester. From the stress-strain curve, the maximal stress (strength) $\pm_{max}$ in was identified and Young's modulus E was determined from the linear section of the stress-strain curve.

DEM analysis

Corn stalk pith consists of spongy parenchyma and vascular bundles *(Thamae Thimothy et al., 2008)*. The vascular bundles embedded into the parenchyma have a small percentage of volume and weight. The external load is carried mostly on the spongy parenchyma. Therefore, CSP could be considered as an isotropic porous material. A discrete spherical particle contacting mechanics model was used to simulate the CSP behaviour. The tissue was represented by spherical particles and the bio-bonding forces between tissues were represented through the contact, friction and damping forces between the particles (Fig.3). The advantages of using the DEM model were to simulate the "porous" nature of CSP and to handle large deformations that CSP might experience in various applications, such as packaging.

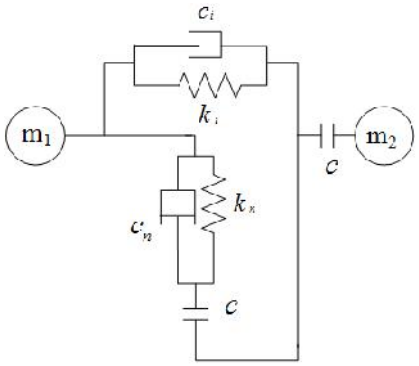

Fig. 3 - Sphere contact model for CSP

Note: k_n and k_s are normal and shear stiffness between two particles (N/m)

c_n and c_s are the normal and shear damping. C is the coupling relation

In the proposed model, inter-particle forces (torques) satisfied the following equilibrium equations *(Itasca, 2008)*:

$$\vec{F} = F_n \vec{n}_n + F_s \vec{n}_s \quad [\text{N}] \tag{1}$$

$$\vec{M} = M_n \vec{n}_n + M_s \vec{n}_s \quad [\text{Nm}] \tag{2}$$

$$F_n = K_n A U_n \quad [\text{N}] \tag{3}$$

$$F_s = K_s A U_s \quad [\text{N}] \tag{4}$$

$$M_n = K_s \bar{J}_n \quad [\text{Nm}] \tag{5}$$

$$M_S = K_n \bar{J}_S \quad [\text{Nm}] \tag{6}$$

In which:

$\vec{F}$, $\vec{M}$ are the inter-particles contacting force and moment;

$\vec{n}_n$, $\vec{n}_s$ are the normal and tangent unit vectors;

F_n, F_s are the normal and tangent forces;

M_n, M_s are the normal and tangent moments;

K_n, K_S are particle normal and tangent stiffness;

U_n, U_S are the normal and tangent displacements, (m);

A is the constraint cross section area, (m^2);

J is the contact surface polar moment of inertia, (m^4);

I is the constraint cross section moment of inertia about axis through contacting point, ($kg.m^2$);

$\bar{}_n$, $\bar{}_s$ are the normal and tangent angular displacements, (rad).

The parameters in the DEM model could not be directly determined from experiments. Therefore, the DEM model was used to simulate the tensile tests and the simulated results were then compared with the experimental results to generate the best-fit DEM model parameters. The simulated CSP had the same geometry and dimensions of the test specimen (Fig. 4).

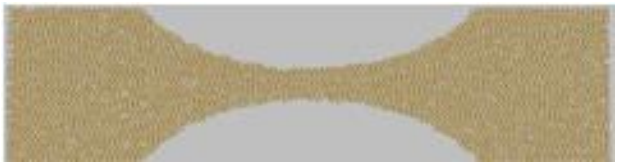

Fig. 4 - Tensile specimen model of CSP

In order to develop a DEM model that closely represented CSP, some critical physical parameters, such as density, had to match the measured value. The corn stalk pith density was determined to be 160-1100 kg/m^3 based on the measured mass and volume. The porosity was calculated as:

$$n = \frac{v_p}{1 - v_p} \tag{7}$$

where n is porosity, and v_p is volume of void, m^3. The simulated density was derived from:

$$\rho = \frac{\rho_1}{n+1} \tag{8}$$

where ρ is simulated particle density, and ρ_1 is the measured pith density.

RESULTS

Experimental results

Figure 5 shows a typical failure pattern of CSP specimens in tensile test. The fracture surface was flat with little shrinkage in the cross-sectional area, which is of typical brittle failure.

Fig.5 - The broken specimen

The measured load-deformation curves showed four distinct stages before the occurrence of failure: initial defamation; linear increase; yield, and fracture. During the initial deformation, elongation was significant at low stress level. This “flat” portion of the load-deformation curve might not reflect the behaviour of CSP; rather, it was due to slip between the specimen and the grips. In the second stage, elongation increased linearly with load. Yielding was identified by a small dip in load. Load continued to increase after yielding until the peak was reached. Finally, fracture occurred and the load began to decrease. The load decreased to zero when the sample was broken completely.

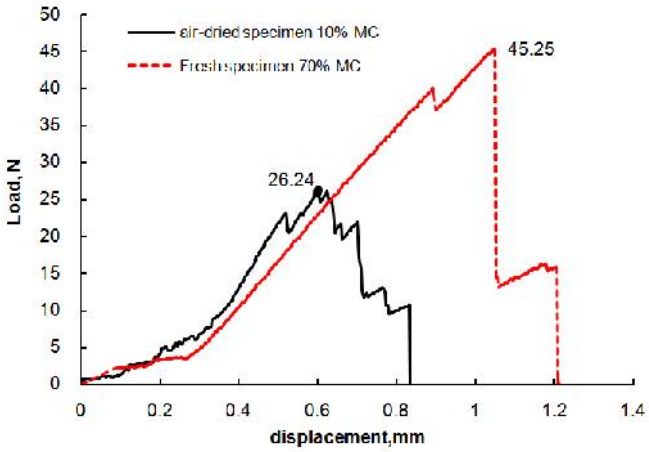

Fig. 6 - Load-displacement curve

The load-deformation curves were noticeably different for CSP specimens of different moisture contents (Fig.6). The fresh specimens at higher moisture content exhibited greater strength and elasticity than did the dried specimens (Fig.6). In the dried specimens, internal voids began to appear due to

shrinkage as the moisture content decreased. Thus, failure could have begun to initiate near the large voids and quickly propagate to the neighbouring areas. This explained why dried CSP specimens were weaker than the fresh specimens.

The tensile strengths of CSP calculated from the measured peak loads are summarized in Figure 7. Analysis of variance showed that dried corn stalk pith had a significantly lower tensile strength than the fresh CSP ($P \leq 0.05$). On the other hand, the internodal position and variety did not have any significant influence on tensile strength ($P > 0.05$). On average, fresh and dry specimens had an average tensile strength of 1.09MPa and 0.86MPa, respectively. The tensile strengths for the two varieties (SD9 and SD 12) of corn stalks were 1.00 MPa and 0.95 MPa, respectively.

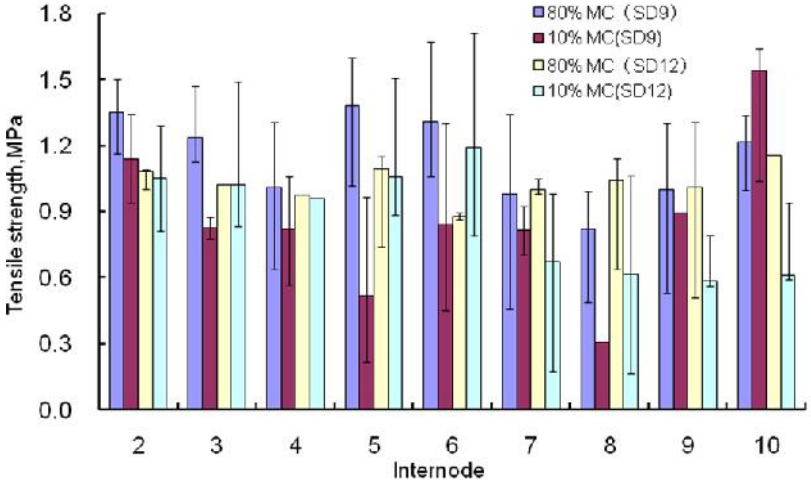

Fig. 7 - Variation of tensile strength of corn stalk pith for different varieties, moisture contents and internodes

Figure 8 summarizes the measured values of Young's modulus for different varieties，moisture contents and internodes. Dried corn stalk pith had a significantly higher Young's modulus (0.12 GPa) than did the fresh samples (0.06 GPa)($P < 0.05$). The internodes position and corn variety did not have any significant influence on the Young's modulus ($P > 0.05$).

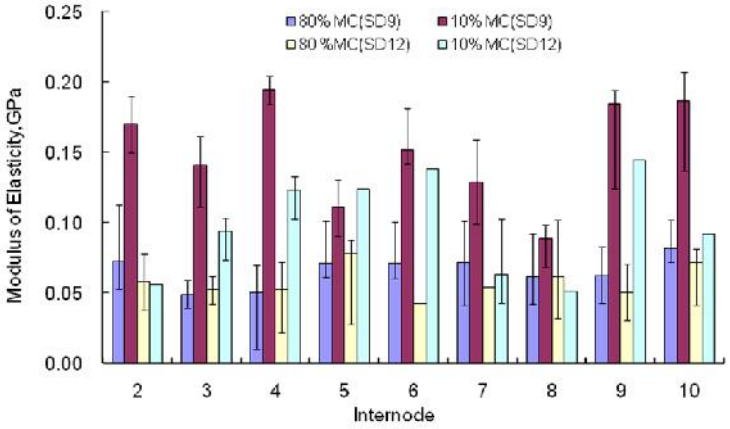

Fig. 8- Variation of elastic of modulus of corn stalk core for different varieties, moisture contents and internodes

Simulation results

After running simulations for all the conditions of tensile test considered in the study, it was found that the particle density had little impact on the simulated mechanical behaviour of CSP in tensile tests. This was attributed to the fact that the gravitational force and applied tensile force were perpendicular to each other in the DEM simulations. The particle radius and porosity significantly impacted the failure pattern (the shape of fracture surface) and computational time. The simulated fracture surface agreed with experimental observations when the number of particles exceeded 5000. When the particle radius and porosity were small ($R < 0.43$mm，$n < 0.35$), the time of model run time was over 40 hours. The range

of particle radius and porosity were optimized based on trial runs of simulation to keep the run time below 24 hours (Table 2).

To determine DEM model mechanical property parameters, including inter-particle normal stiffness coefficient K_n, tangential stiffness coefficient K_s, normal bonding coefficient, tangential bonding coefficient and friction coefficient « , simulations were conducted for a range of parameter values and the correlations between the these parameters and the simulated strength were developed in Equation (9):

$$\left.\begin{aligned} y_1 &= 18.247x_1^3 - 102.13x_1^2 + 171.26x_1 + 51.52(R^2 = 1) \\ y_2 &= 181.59e^{-0.233x_2}(R^2 = 0.9202) \\ y_3 &= 2.9147x_3 - 3.2878(R^2 = 0.9882) \\ y_4 &= -0.0051x_4^3 + 0.442x_4^2 - 10.77x_4 + 209.9(R^2 = 1) \end{aligned}\right\} \quad (9)$$

Where:

x_1 is the tangential stiffness coefficient;

x_2 is the normal stiffness coefficient;

x_3 is the normal bonding coefficient;

x_4 is the tangent bonding coefficient;

y_i is the ultimate strengths.

Simulation shows that normal bonding coefficient x_3 had a significant influence (R>0.05) to strength, while the other factors had no impact (R<0.05). The model's macro-mechanical behaviours (e.g., cross section shape, location and number of overflow particles) also would be change with the parameters value. The optimized range of x_1, x_2, x_3 and x_4 were determined by comparing the model's macro-mechanical behaviours and the experimental phenomenon:

$$\left.\begin{aligned} x_1, x_2 &\in (0.5\text{E+}06, 3\text{E+}06) \\ x_3 &\in (5, 50) \\ x_4 &\in (10, 50) \end{aligned}\right\} \quad (10)$$

The obtained numerical values of the best-fit DEM model parameters are summarized in Table 2. It was impossible to match the simulated results with the experimental data with a single set of DEM model parameters. Therefore, the ranges of parameters values were determined, and two simulation models were then created – Model 1 was based on the lower limits of parameter ranges, and Model 2 on the upper limits (Table 2).

Table 2

Numerical range of particles' mechanical parameters

Parameter	value
Sphere particle density/kg·m^{-3}	753
Sphere particle radius/mm	0.43-0.5
Porosity/kg·m^{-3}	0.35-0.65
k_n / N·m^{-1}	0.5E+06-1.5 E+06 (model 1)
	2 E+06-3.0 E+06 (model 2)
k_S / N·m^{-1}	1.0 E+06
n – bond / N·m^{-3}	5-30 (model 1)
	35-50 (model 2)
s – bond / N·m^{-3}	10-20 (model 1)
	40-50 (model 2))
Friction coefficient	1

The simulated responses of CSP (e.g. contacting force chain and fracture lines) are visualized in Fig.9. The left end was the fixed boundary and the right end was moved at a speed of 5 mm/min (the loading rate used in the tensile tests). It was visible that voids occurred as the loading progresses. The lines in the diagram represent the force chains. It is intersecting to note that forces (stresses) were not transmitted uniformly in the simulated CSP. The maximum stress and fracture would occur in the area where force transmission lines were intensely populated.

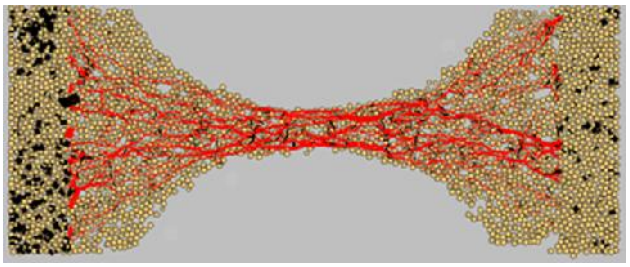

Fig. 9 - Simulated force transmission in a specimen of tensile test

As the load was increasing, the voids became larger, causing reductions in the actual cross-sectional area for carrying the load; the specimen was broken when the stress at a critical location exceeded the ultimate bonding strength between particles. The fractured cross section tended to be flat, as shown in Figure 10, which was similar to that observed in the experiments (Fig. 5).

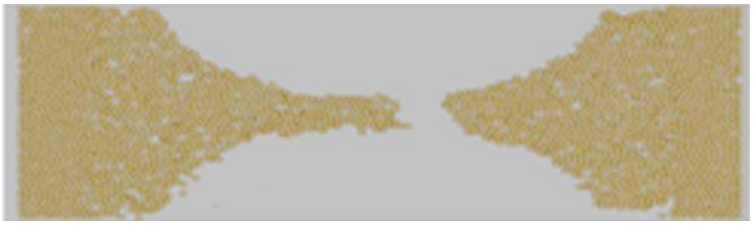

Fig. 10 - Simulated fracture surface of CSP specimen

Simulated load-displacement curves similar to the measured curves (Figs.11 and 6). However, the strength results differed – the simulated strength was found to be approximately 2.3-17.9 times the real strength. For example, an ultimate load 138.48 N was predicted by Model 1 (Fig.10), whereas a load of 45.25 N was measured for the fresh specimen (Fig.3). The parameters of the micro mechanical properties correspond to the macro parameters, which indicate that the micro mechanical properties matched well with the properties of corn stalk pith.

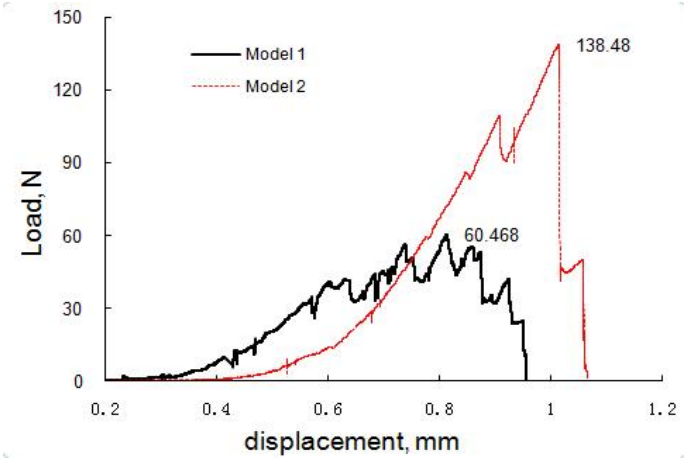

Fig. 11 - Load-displacement curves simulated with DEM model

Using smaller values of model parameters (Table 3), Model 1 resulted in lower strength and stiffness, which led to further local failure and dramatic stress changes, in comparison with Model 2, which used greater values of property parameters.

Table 3

The value of particles' mechanical parameters in model 1 and model 2

Parameter	model 1	model 2
Sphere particle density / N·m^3	753	753
Sphere particle radius / mm	0.5	0.5

Parameter	model 1	model 2
Porosity / $N \cdot m^3$	0.65	0.65
k_n / $N \cdot m^{-1}$	1.50E+06	2.00E+06
k_s / $N \cdot m^{-1}$	1.00E+06	1.00E+06
$n-bond / N \cdot m^{-3}$	10	50
$s-bond / N \cdot m^{-3}$	10	50

CONCLUSIONS

A tensile test and DEM simulation were conducted to investigate the tensile strength and Young's modulus for different varieties of corn stalk pith under various conditions. The influence of moisture content, internodal position and variety on corn stalk pith's tensile strength and Young's modulus was analysed. The main conclusions in this paper are:

(1) Load-displacement curves in tensile tests indicated that both fresh and dry corn stalk pith fractured as a brittle material.

(2) Fresh corn stalk pith had greater tensile strength, but lower Young's modulus than the dry corn stalk.

(3) The internodes position and corn variety had insignificant effect on either the tensile strength or Young's modulus of fresh and dry corn stalk pith.

(4) The optimized DEM model parameters for dry corn stalk pith were: K_n = (0.5-1.5)x10^6 N/m, K_s= 1.0x10^6 N/m, n-bond=(5-30) N/m^3 and s-bond=(10-20) N/m. For fresh stalk they were: K_n = (2.0-3.0)x10^6 N/m, K_s = 1.0x10^6 N/ m, n-bond = (35-50) N/m^3 and s-bond = (40-50) N/m^3.

(5) The shape of load-displacement curves simulated with the DEM was similar to the measured curves; The simulated ultimate strength was approximately 2.3-17.9 times that of the measured values.

The corn stalk pith material model developed by utilizing both tensile test results and DEM analysis was simplified and found to match the real material; therefore, in our opinion, this model is capable of providing valuable data for further investigation.

ACKNOWLEDGEMENT

This work was supported in part by The Public Welfare and Industry Special Fund Project of the Ministry of Agriculture of China: Crop straw substrate utilization (201503137).

REFERENCES

[1] Asbe A., (2006). S358. 2: *Moisture Measurement-Forages*. ASAE Standards, USA.

[2] Chen Z., (2012). Experiment on tensile and shearing characteristics of rind of corn stalk. *Transactions of the Chinese Society of Agricultural Engineering*, Beijing/China, Vol. 28, Issue 21, pp. 59-65;

[3] Cundall P. A., (1988). Formulation of a three-dimensional distinct element model—Part I. A scheme to detect and represent contacts in a system composed of many polyhedral blocks. *Paper presented at the International Journal of Rock Mechanics and Mining Sciences & Geomechanics Abstracts*, Oxford/England, Vol. 25, Issue 3, pp.107-116;

[4] Hart R., (1988). Formulation of a three-dimensional distinct element model—Part II. Mechanical calculations for motion and interaction of a system composed of many polyhedral blocks. *International Journal of Rock Mechanics & Mining Science & Geomechanics Abstracts*, Oxford/England, Vol. 25, Issue 3, pp.117-125;

[5] Hu H., (2013). QTL mapping of stalk bending strength in a recombinant inbred line maize population. *Theor Appl Genet*, Beijing/China, Vol. 126, Issue 9, pp. 2257-2266;

[6] Husseien M., (2009). A comprehensive characterization of corn stalk and study of carbonized corn stalk in dye and gas oil sorption. *Journal of Analytical and Applied Pyrolysis*, Amsterdam/Netherlands, Vol. 86, Issue 2, pp. 360-363;

[7] Igathinathane C., (2010). Corn stalk orientation effect on mechanical cutting. *Biosystems Engineering,* San Diego/USA ,Vol. 107, Issue 2, pp. 97-106;

[8] Itasca, (2008). *PFC3D particle flow code in 3 dimensions, theory and background.* Inc. Minneapolis.
[9] Li Z., (2012). Cell morphology and chemical characteristics of corn stover fractions. *Industrial Crops and Products*, Amsterdam/Netherlands, Vol. 37, Issue 1, pp. 130-136;
[10] Liao Na., (2011). Structure Modeling and Radial Compression Simulation of Corn Stalk Cores *Transactions of the Chinese Society for Agricultural Machinery*, Beijing/China, Vol. 42, Issue 6, pp. 117-121;
[11] Nazari Galedar M., et al., (2008). *Effects of moisture content and level in the crop on the engineering properties of alfalfa stems. Biosystems Engineering*, San Diego/USA, Vol. 101, Issue 2, pp.199-208;
[12] Panthapulakkal S., (2007). Agro-residue reinforced high-density polyethylene composites: Fibre characterization and analysis of composite properties. *Composites Part A: Applied Science and Manufacturing*, Oxford/England, Vol. 38, Issue 6, pp. 1445-1454;
[13] Peiffer J. A., (2013). The genetic architecture of maize stalk strength. *PLoS One,* Cambridge/United Kingdom Vol. 8, Issue 6, pp.66-67.
[14] Qin C., (2013). Impact splitting tensile experiments of concrete and numerical modeling by meso-scale discrete elements. *Journal of Hydroelectric Engineering,* Beijing/China, Vol. 32, Issue 1, pp.196-205;
[15] Reddy N., (2005). Structure and properties of high quality natural cellulose fibres from cornstalks. *Polymer*, Oxford/England, Vol. 46, Issue 15, pp. 5494-5500;
[16] Rodriguez M., (2010). Determination of corn stalk fibres' strength through modeling of the mechanical properties of its composites. *BioResources*, Raleigh/USA, vol. 5, Issue. 4, pp. 2535-2546;
[17] Rousserie F., (1997). Characterization of corrugated board panels: an experimental study. *Journal of pulp and paper science*, Montreal/Canada, Vol. 23, Issue 7, pp. 330-334;
[18] Speck T., (2011). Plant Stems: Functional Design and Mechanics. *Annual Review of Materials Research,* Palo Alto/USA, Vol. 41, Issue 1, pp.169-193;
[19] Standard test methods and definitions for mechanical testing of steel products. (2014). Astm. http://xueshu.baidu.com/s?wd=paperuri%3A%28dad744dd4d6f60d54b4bd89236f0fd16%29&filter=sc_long_sign&tn=SE_xueshusource_2kduw22v&sc_vurl=http%3A%2F%2Fcds.cern.ch%2Frecord%2F2031231&ie=utf-8&sc_us=16224858868936973418
[20] Tavakoli H., (2009). Physical and mechanical properties of wheat straw as influenced by moisture content*. Int. Agrophysics*, Lublin/Poland, Vol. 23, Issue 2, pp.175-181;
[21] Thamae T., (2008). Developing and characterizing new materials based on waste plastic and agro-fibre. *Journal of Materials Science*, New York/USA ,Vol. 43, Issue 12, pp. 4057-4068;
[22] Von Forell G., (2015). Preventing lodging in bioenergy crops: a biomechanical analysis of maize stalks suggests a new approach*. Journal of experimental botany*, Oxford/England, Vol. 66, Issue 14, pp.4367;
[23] Wang D., (2002). Low density particleboard from wheat straw and corn pith. *Industrial Crops & Products*, Amsterdam/Netherlands, Vol.15, Issue 1, pp. 43-50;
[24] Wright C.T., (2005). Biomechanics of wheat/barley straw and corn stover. *Applied biochemistry and biotechnology*, Totowa/USA, Vol. 121, Issue 1-3, pp. 5-19;
[25] Zhang L., (2016). Tensile Properties of Maize Stalk Rind. *BioResources,* Raleigh/USA, Vol. 11, Issue 3, pp. 6151-6161.
[26] Zhong-Zhen S., (2013). The Viscoelasticity Model of Corn Straw under the Different Moisture Contents. *Mathematical Problems in Engineering,* Totowa/USA, Vol. 2013, Issue 6, pp. 14-26.